



HAL
open science

Transverse beam emittance studies of the CYRCé TR24 cyclotron

E. Bouquerel, E. Traykov, K.P. Nesteruk, S. Braccini, T.S. Carzaniga, C. Mathieu, M. Pellicoli, M. Rousseau, C. Ruescas, J. Schuler, et al.

► **To cite this version:**

E. Bouquerel, E. Traykov, K.P. Nesteruk, S. Braccini, T.S. Carzaniga, et al.. Transverse beam emittance studies of the CYRCé TR24 cyclotron. Nuclear Instruments and Methods in Physics Research Section A: Accelerators, Spectrometers, Detectors and Associated Equipment, 2019, 931, pp.151-157. 10.1016/j.nima.2019.04.028 . hal-03444706

HAL Id: hal-03444706

<https://hal.science/hal-03444706v1>

Submitted on 20 Dec 2021

HAL is a multi-disciplinary open access archive for the deposit and dissemination of scientific research documents, whether they are published or not. The documents may come from teaching and research institutions in France or abroad, or from public or private research centers.

L'archive ouverte pluridisciplinaire **HAL**, est destinée au dépôt et à la diffusion de documents scientifiques de niveau recherche, publiés ou non, émanant des établissements d'enseignement et de recherche français ou étrangers, des laboratoires publics ou privés.



Distributed under a Creative Commons Attribution - NonCommercial 4.0 International License

Transverse beam emittance studies of the CYRCé TR24 cyclotron

E. Bouquerel^{a,*}, E. Traykov^a, K. P. Nesteruk^{b,1}, S. Braccini^b,
T. S. Carzaniga^b, C. Mathieu^a, M. Pellicoli^a, M. Rousseau^a, C. Ruescas^a,
J. Schuler^a, S. Vichi^{b,c}

^a*IPHC, UNISTRA, CNRS, 23 rue du Loess, 67200 Strasbourg, France*

^b*Albert Einstein Center for Fundamental Physics (AEC),
Laboratory for High Energy Physics (LHEP), University of Bern,
Sidlerstrasse 5, CH-3012 Bern, Switzerland*

^c*Department of Industrial Engineering, University of Bologna, Viale del Risorgimento 2,
40136 Bologna, Italy*

Abstract

The PRECY project foresees the use of a 16-25 MeV energy proton beam produced by the TR24 cyclotron, named CYRCé, recently installed at the Institut Pluridisciplinaire Hubert Curien (IPHC) in Strasbourg for research in radiation biology. One of the exit ports of the cyclotron will be used for this application along with a combination magnet. The platform will consist of up to 5 experimental stations linked to beamlines located in a dedicated area next to the cyclotron vault. One of the beamlines will receive proton beams of a few cm diameter at intensities up to 100 nA. In order to characterize the beam extracted from the cyclotron, the transverse beam emittance was studied by means of different methods.

Keywords: Beam emittance, Diagnostics, Cyclotron

1. Introduction

The Institut Pluridisciplinaire Hubert Curien (IPHC/CNRS) in Strasbourg recently inaugurated its brand new circular accelerator manufactured by ACSI [1]. This cyclotron, called CYRCé, works at energies between 16 and 25 MeV with

*Corresponding author

Email address: elian.bouquerel@iphc.cnrs.fr (E. Bouquerel)

¹Currently at Paul Scherrer Institut, Switzerland

18 intensities up to 500 μA . It can produce radioisotopes for positron emission to-
19 mography (PET) (^{11}C , ^{13}N , ^{15}O , ^{18}F , ^{124}I , ^{64}Cu , ^{68}Ge , ^{76}Br , ^{89}Zr) and for single-
20 photon emission computed tomography (^{123}I , ^{111}In , ^{67}Ga , ^{57}Co , ^{99m}Tc). Re-
21 cently a new project arose with the aim of developing a Platform for Radiobio-
22 logical Experiments using protons produced by CYRCé (PRECy). This project
23 is driven by a collaboration of physicists and biologists. Its objective is to allow
24 a better understanding of the effect of proton radiation on the living matter.
25 The specificity of the PRECy project at the national and European level is
26 based on its interconnection with the various existing platforms and equipment
27 at the IPHC (preclinical molecular imaging, proteomics based on mass spec-
28 trometry analysis, cell and molecular biology laboratory, pet shop, and animal
29 physiology and behavior laboratory) making a unique place for the development
30 of multiparametric and macroscopic studies of tumor evolution in vitro and in
31 vivo in small animals. The development of one or several beamlines is foreseen.
32 The first beamline will deliver macro beams of 1 to 2 cm diameter at intensities
33 up to 100 nA. To design and define the optical elements mandatory to trans-
34 port beam efficiently through this beamline, the proton beam delivered from
35 the cyclotron has to be accurately characterized. Along this line, the transverse
36 beam emittance is a parameter of paramount importance. Several techniques
37 of emittance measurements are known and have been successfully tested in the
38 past, e.g. techniques based on foil irradiation [2, 3]. This paper presents three
39 different techniques that have been used to determine the transverse emittances
40 of the beam extracted from CYRCé.

41 **2. Quadrupole variation method**

42 The quadrupole variation method, uses the combination of quadrupole(s)
43 together with profilers [4]. In this technique, the emittance value is obtained
44 from the correlation between the beam size and the quadrupole magnetic field
45 in the transformation matrix model. Assuming the following transformation
46 matrix R:

$$R = \begin{pmatrix} R_{11} + KR_{12} & R_{12} \\ R_{21} + KR_{22} & R_{22} \end{pmatrix}$$

47 and the transfer matrix of the quadrupole Q:

$$Q = \begin{pmatrix} 1 & 0 \\ K & 1 \end{pmatrix}$$

the resultant matrix taking into account the beam parameter is:

$$\begin{aligned} \sigma_{11}(z) = & (\sigma_{11}(z_0)R_{11}^2 + 2\sigma_{12}(z)R_{11}R_{12} + \sigma_{22}(z_0)R_{12}^2) \\ & + (2R_{11}R_{12}\sigma_{11} + 2R_{12}^2\sigma_{12})K + R_{12}^2\sigma_{11}(z_0)K^2 \end{aligned}$$

48 A quadrupole scan consists of a set of N beam profile measurements at a
 49 fixed distance from the quadrupole magnet, as the quadrupole field strength is
 50 varied over a range of values. Plotting each of the beam size with respect to
 51 the quadrupole strength gives a parabolic curve from which the emittance and
 52 phase space parameters are extracted. From the fitting process of the parabolic
 53 curve the following values are determined:

$$\begin{aligned} 54 \quad A &= R_{12}^2\sigma_{11}(z_0); \\ 55 \quad -2AB &= 2R_{11}R_{12}\sigma_{11} + 2R_{12}^2\sigma_{12}; \\ 56 \quad C + AB^2 &= \sigma_{11}(z_0)R_{11}^2 + 2\sigma_{12}(z)R_{11}R_{12} + \sigma_{22}(z_0)R_{12}^2 \end{aligned}$$

57 The determination of the A, B, C coefficients allows finding the Twiss pa-
 58 rameters β , α and γ and the corresponding transverse emittance [4]. As shown
 59 in Fig. 1, the experimental setup consisted of a doublet of quadrupoles (QA,
 60 QB) and 2 beam profilers positions (Diag1, Diag2). The beam profiler, a single-
 61 wire scanner, was designed and built at the IPHC (Fig. 2). It consists of two
 62 piezoelectric displacement axes: translation and rotation. Table 1 presents the
 63 characteristics of the positioning. The wire, made of tungsten, has a thickness
 64 of 0.5 mm and is fixed to a Teflon support. The beam deposits its charge on
 65 the wire and the current is measured (orders of pA minimum) using a Keithley

Table 1: characteristics of the scanning wire.

Travel	± 20.05 (41) mm
Step width	1 - 1.500 nm
Scan range	≥ 1.5 μm
Scan resolution	≤ 1 nm
Velocity	≥ 20 mm/s
Max. frequency	18.5 kHz

66 device [5]. The quadrupoles have an aperture of ± 39 mm, a maximum field
67 gradient of 9.3 T/m and a magnetic length of 297 mm each. The doublet was
68 positioned at a distance of 154.5 mm from the switching dipole (Dip1) located
69 just after the exit of the cyclotron. Profilers were located at 570 mm and 1690
70 mm away from the center of the doublet. The polarity of each of the quadrupoles
71 was reversed during the tests, which gave a total number of 8 sets of values while
72 varying the field gradients. Measurements were performed for protons at kinetic
73 energies of 25 MeV and at a constant beam intensity of 25 nA.

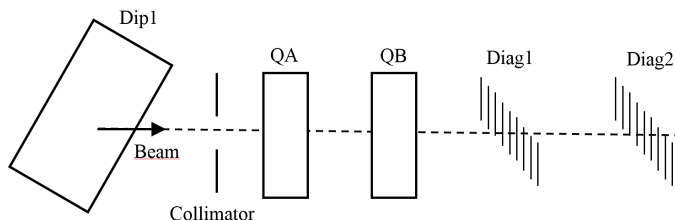


Figure 1: Schematic view of the quadrupole variation method and the different optical elements for the emittance measurement. Dip1 is the dipole at the exit of the cyclotron, QA and QB are quadrupoles, Diag1 and Diag2 are the profiler's positions.

74 The intensity of the beam was measured as a function of the current in
75 the coils of the quadrupoles QA or/and QB. The main objective was to find
76 the set up values in each configuration which gives a waist to the beam at the
77 profilers location. Fig. 3 shows the variation of the particle density according
78 to the quadrupole fields at a proton energy of 25 MeV. In this example, QA was

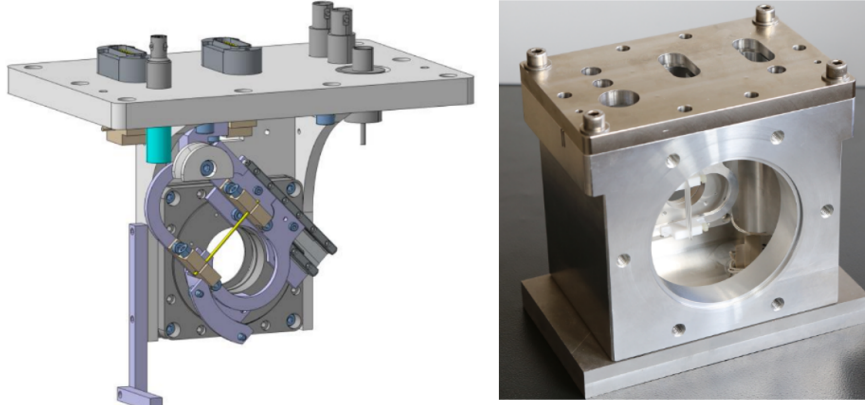


Figure 2: 3D view (left) and picture (right) of the single-wire scanner.

79 focussing in the x axis and QB in the y axis.

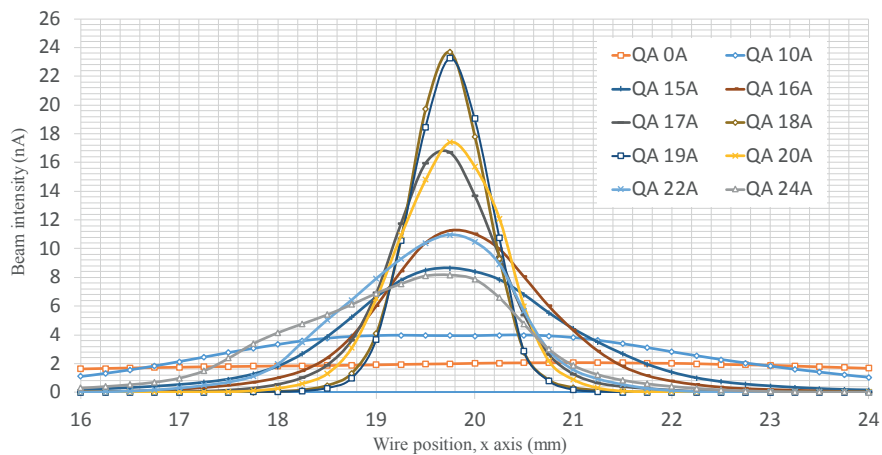


Figure 3: Beam intensities measured on the first profiler (Diag1) according to the intensity in the coils of the quadrupoles QA. $I(QB) = 0A$. Proton at 25 MeV. Beam waist measured when $I(QA)=18A$.

80 From the quadratic functions (Fig. 4), the emittance-related coefficients
 81 were calculated. Some difficulties with beam alignment and centering at the
 82 quadrupole positions were encountered during the measurements influencing
 83 the results. Therefore, several combinations of dipole settings and foil positions
 84 were used during the measurements. Moreover multiple peak structures were

85 observed in the horizontal profiles contributing to large uncertainties in the
 86 estimated values. The origin of the latter is considered to be associated with
 87 beam extraction from multiple orbits in the cyclotron. The emittances were
 88 measured to be:

89 $\epsilon_x^{rms} = 1.9 \pm 1.3 \pi \cdot \text{mm} \cdot \text{mrad}$ and $\epsilon_y^{rms} = 3.7 \pm 1.4 \pi \cdot \text{mm} \cdot \text{mrad}$.

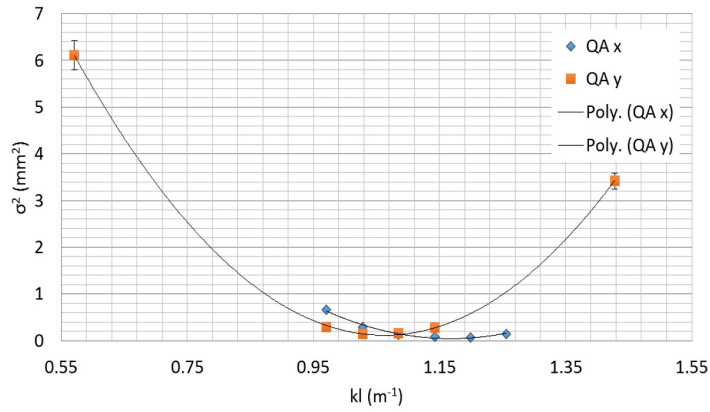


Figure 4: Beam size values according to the strength of the quadrupole QA (Diag1), 25 MeV.

90 3. Method based on a slit and a beam profiler

91 The trasverse beam emittance was also assessed by using a movable slit and
 92 a single wire position scanner profiler. Fig. 5 shows the principle of this method.
 93 The angle x_0 is determined with a multi-wire harp profiler. In the field-free drift
 94 space the trajectories of the particles, combined in a 'beamlet', are straight lines.
 95 The contribution to the emittance plot in the phase space is given by the angle
 96 distribution at the slit location. The slit position is then scanned through the
 97 beam to get all positions. The data have to be normalized to a constant beam
 98 current as measured. After making the full scan, the X-X' ellipse is plotted and
 99 the rms-value of the emittance is calculated from the data. The resolution for
 100 the space coordinate Δx is limited by the slit width $\Delta x = d_{slit}$.

101 The harp profiler consisted of two frames with 48 Tunsten wires with a
 102 thickness of $150 \mu\text{m}$ each ($2r_{wire}$), installed in a flat feedthrough on the rod of

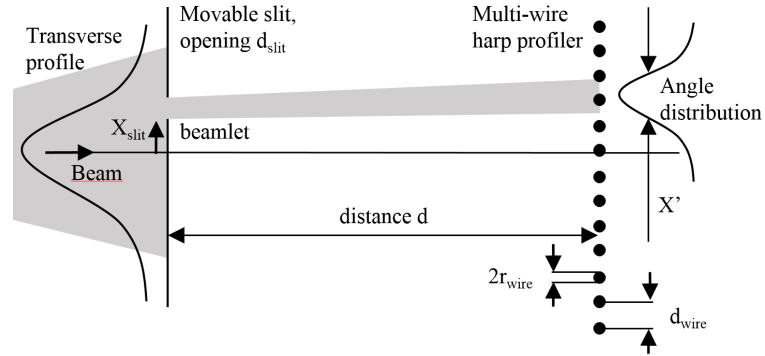


Figure 5: Moving slit technique. The width of the slit d_{slit} gives the resolution in space $\Delta x = d_{slit}$ and the angular resolution is $\Delta x' = (d_{slit} + 2 r_{wire})/d$.

103 pneumatic actuator with a long stroke of 300 mm (Fig. 6). The drive design
 104 allows precise alignment of the detector with respect to the beam axis. The
 105 entire mechanical system was assembled on a mounting flange.

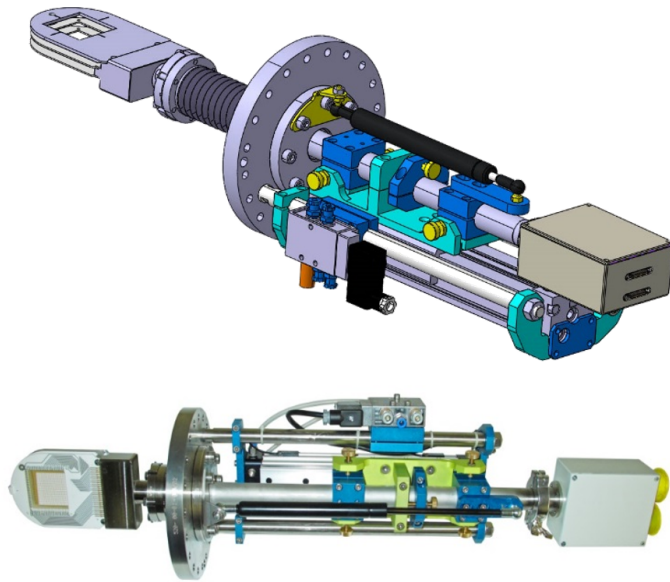


Figure 6: 3D view (top) and picture (bottom) of the multi-wire profiler.

106 The measurement of the signal from the wire is done by integrating the

107 charge over a certain period of time. Varying the integration time allows chang-
 108 ing the dynamic range of the profilometer over a wide range and choosing the
 109 most optimal value based on the beam parameters. The integration time can
 110 be set from 1 ms to several seconds. To collect the charge on each wire, 0.2 nF
 111 capacitors are used. The average current on the wire is determined by the value
 112 of the voltage on the capacitor. The main electronics module used includes
 113 two sections of 48 channels each, a power supply with an output voltage of 15
 114 volts and an additional unit with a voltage of 100 volts to power the collecting
 115 electrodes. The data set interface allowed to visualize the measured vertical
 116 and horizontal beam profiles, as well as the values of their center of gravity and
 117 width.

118 The distance between the wires, d_{wire} , was 1 mm. The size of the slit,
 119 d_{slit} , was 200 μm . For the measurement, the doublet was kept positioned at a
 120 distance of 154.5 mm from the switching dipole located just after the exit of the
 121 cyclotron. The profiler was set a distance of 169 mm away from the doublet of
 122 quadrupoles. The angular resolution of the system, defined by
 123 $\Delta x' = (d_{slit} + 2 r_{wire}) / d$, was 0.30 mrad.

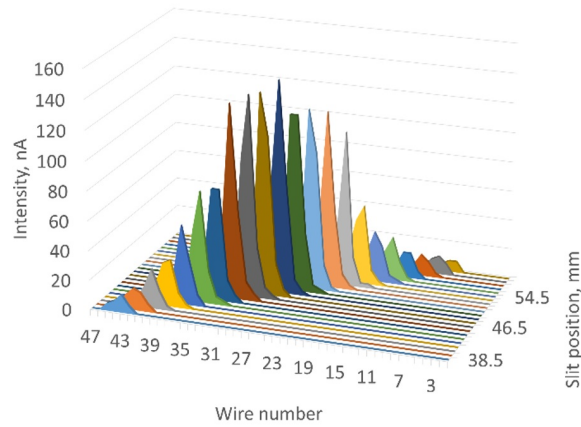


Figure 7: Intensity measured on the wires of the grid (vertical position) for proton energy of 25 MeV. Figure in colour

124 Fig. 7 shows an example of the set of data measured while the slit is in

125 the vertical position. The intensity of the beam was kept constant at 120 nA
 126 during the measurement process. An additional estimation of the transverse
 127 emittances was performed by using TraceWin [6] in order to verify the results
 128 obtained by the slit-and-grid method. Indeed, the beam distributions were
 129 reproduced in the code and the input beam parameters used in the simulations
 130 were adjusted to achieve matching between the simulated and the measured
 131 profiles. This allowed to make an estimation both of the emittances and the
 132 upstream beam parameters (after the dipole). Fig. 8 and 9 show the beam
 133 output distributions implemented in Tracewin from the experimental data at
 134 the profiler location and the distributions simulated with TraceWin respectively.
 135 From these analyses, transverse emittance was estimated at 25 MeV:
 136 $\epsilon_x^{rms} = 1.4 \pm 0.2 \pi \cdot \text{mm} \cdot \text{mrad}$ and $\epsilon_y^{rms} = 5.4 \pm 0.2 \pi \cdot \text{mm} \cdot \text{mrad}$.

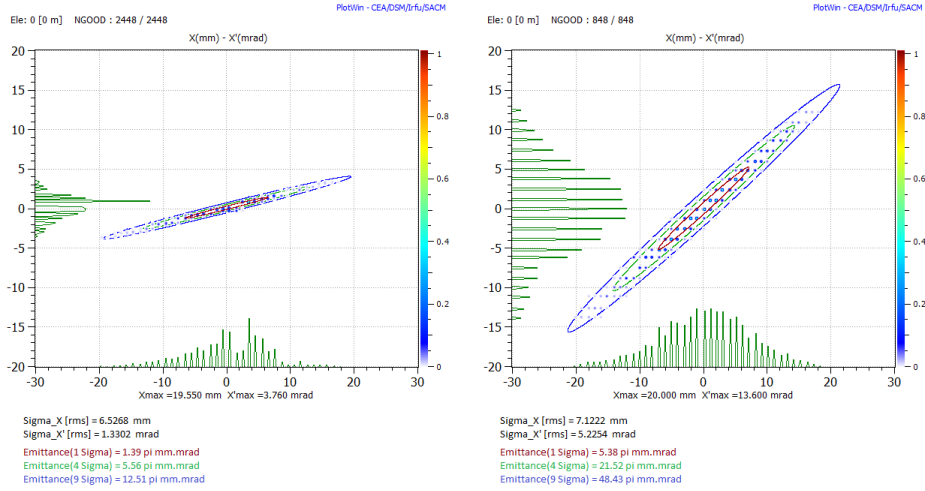


Figure 8: Beam output phase-space distribution in xx' and yy' from experimental data. Figure in colour.

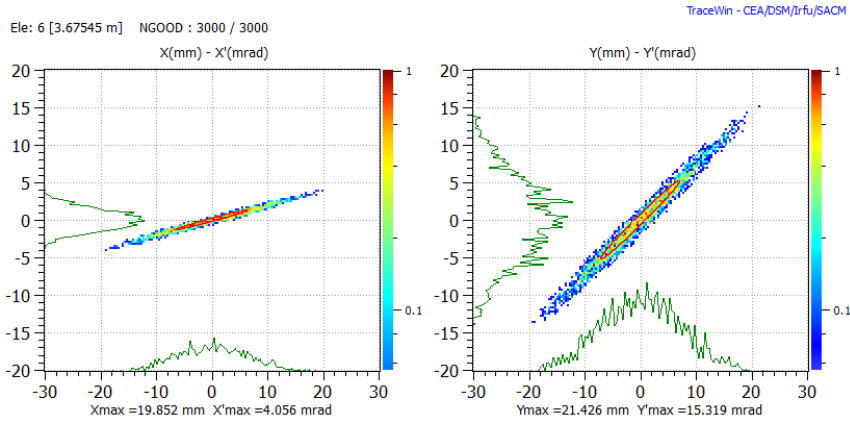


Figure 9: Beam output phase-space distribution in xx' and yy' from simulation. Figure in colour.

137 4. Multiple beam profiler technique

138 A system for online measurement of the transverse beam emittance has been
 139 developed at the AEC-LHEP of the University of Bern and is described in [7].
 140 The system, named ${}^4\text{PrOB}\epsilon\text{aM}$, consists of four UniBEaM beam monitors, also
 141 conceived and built at AEC-LHEP [8, 9]. The UniBEaM detector is based on
 142 a single scintillating fiber moved across the beam. When a charged particle
 143 passes through the fiber, light is produced and transported through a standard
 144 multi-mode optical fiber to a read-out device. There the signal is digitized and
 145 plotted online as a function of the fiber position. The signal measured by the
 146 UniBEaM profiler is linear with respect to the beam current over a wide range
 147 from 1 pA to about $3 \mu\text{A}$ [8].

The ${}^4\text{PrOB}\epsilon\text{aM}$ system allows the transverse beam emittance to be measured in each plane in a fraction of a minute. It uses the multipole beam profiler method [10]. Beam profiles are measured at four locations along a beamline, as shown in Fig. 10. For each of them, the variance (RMS^2) and its uncertainty are calculated giving an estimate of $\sigma_{11}(s)$ component of the beam matrix $\sigma(s)$ at the location s , as depicted in Fig. 11. The beam transfer matrix $R(s)$ involves



Figure 10: The ${}^4\text{PrOB}\epsilon\text{aM}$ system installed on the research beamline of the TR24 cyclotron in Strasbourg. Four UniBEaM beam profilers are visible.

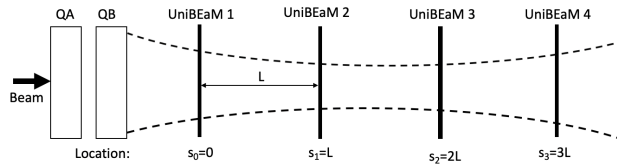


Figure 11: Sketch of principle of the multiple beam profiler method for the measurement of the transverse beam emittance.

only a drift:

$$R(s) = \begin{pmatrix} 1 & s \\ 0 & 1 \end{pmatrix}$$

The beam matrix at any location s with respect to the location of the first profiler ($s_0 = 0$) is therefore given by the formula:

$$\sigma(s) = R(s)\sigma(0)R(s)^T$$

From the equation above it can be derived that $\sigma_{11}(s)$ is a quadratic function

of s :

$$\begin{aligned}\sigma_{11}(s) &= \sigma_{22}(0)s^2 + 2s\sigma_{12}(0) + \sigma_{11}(0) \\ &= f(s; \sigma_{11}(0), \sigma_{12}(0), \sigma_{22}(0)),\end{aligned}$$

148 where $\sigma_{11}(0)$, $\sigma_{12}(0)$, and $\sigma_{22}(0)$ are the components of the $\sigma(0)$ matrix. These
149 components and consequently the transverse RMS emittance $\epsilon^{rms} = \pi\sqrt{\det(\sigma(0))}$
150 are evaluated by fitting the $f(s; \sigma_{11}(0), \sigma_{12}(0), \sigma_{22}(0))$ function using the four
151 data points representing the estimated variance values as a function of the lo-
152 cation s , as shown in Fig. 12.

153 The emittance measurements of the TR24 cyclotron in Strasbourg were con-
154 ducted at the research beamline. The beam current of 10 nA was kept through-
155 out the measurements and was monitored by means of a Faraday cup installed
156 at the end of the beamline. The RMS transverse beam emittance was evalu-
157 ated in both the horizontal and vertical planes at the two most frequently used
158 beam energies of 18 MeV and 25 MeV. Proton beams resulting from the TR24
159 cyclotron are produced by stripping accelerated H^- ions. The stripper angle
160 can be adjusted to optimize the extracted proton beams. For each beam en-
161 ergy, measurements were repeated for different stripper positions to evaluate
162 the sensitivity of the emittance to changes of the stripper azimuthal angle.

163 The results of the emittance measurements for different stripper positions are
164 shown in Figs. 13 and 14 for beam energies of 18 MeV and 25 MeV respectively.
165 The stripper positions chosen are those which are used most often at IPHC
166 and are given by a numerical parameter. For 18 MeV protons, the horizontal
167 emittance was found to be in the range of $(5.01 \pm 0.28) \pi \cdot \text{mm} \cdot \text{mrad}$ to $(5.81 \pm$
168 $0.48) \pi \cdot \text{mm} \cdot \text{mrad}$. The vertical emittance varied from $(5.04 \pm 0.17) \pi \cdot \text{mm} \cdot \text{mrad}$
169 to $(6.94 \pm 0.19) \pi \cdot \text{mm} \cdot \text{mrad}$. For 25 MeV protons, the dependence on the stripper
170 position is weaker. This, however, could be due to the different range in which
171 the stripper angle was changed. In the horizontal plane, the emittance varied
172 from $(2.79 \pm 0.21) \pi \cdot \text{mm} \cdot \text{mrad}$ to $(3.03 \pm 0.22) \pi \cdot \text{mm} \cdot \text{mrad}$, while in the vertical
173 one from $(5.76 \pm 0.18) \pi \cdot \text{mm} \cdot \text{mrad}$ to $(5.96 \pm 0.16) \pi \cdot \text{mm} \cdot \text{mrad}$.

174 The measured value of the vertical RMS beam emittance was always larger

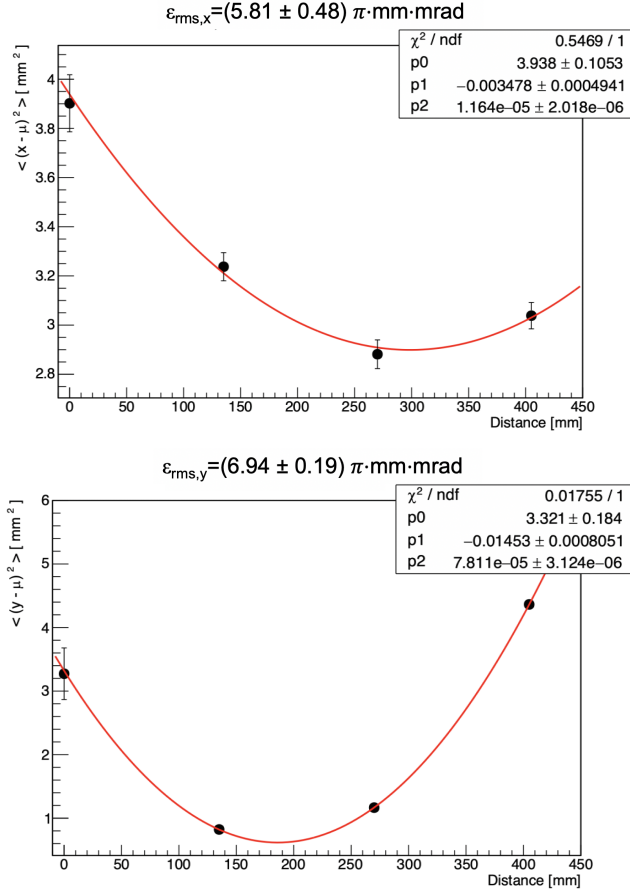


Figure 12: Variance of transverse beam profiles as a function of the location obtained for the horizontal (top) and vertical (bottom) planes.

175 than the corresponding value of the horizontal one. This is probably due to the
 176 axial injection of H^- ions from the external ion source. Acceleration from the
 177 injection point to the extraction stripper is realized in the horizontal plane, and
 178 therefore the axially injected ions must be deflected by 90 degrees, which leads
 179 to emittance growth in the vertical plane.

180 In conclusion, the upper limits of the beam emittance for the 18 MeV proton
 181 beam were found to be $(5.81 \pm 0.48) \pi \cdot \text{mm} \cdot \text{mrad}$ and $(6.94 \pm 0.19) \pi \cdot \text{mm} \cdot \text{mrad}$
 182 for the horizontal and vertical planes, respectively.

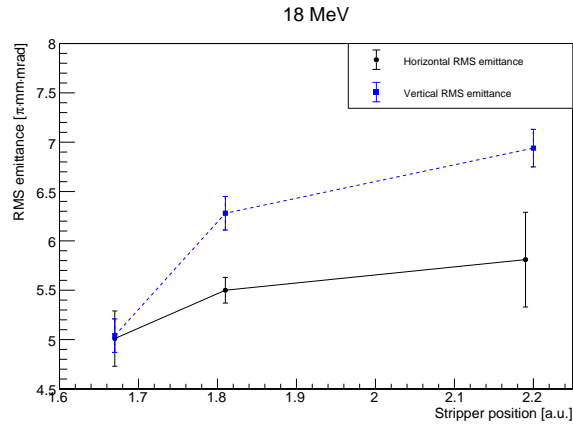


Figure 13: The RMS transverse beam emittance of the 18 MeV proton beam of the TR24 Strasbourg cyclotron as a function of stripper angular position.

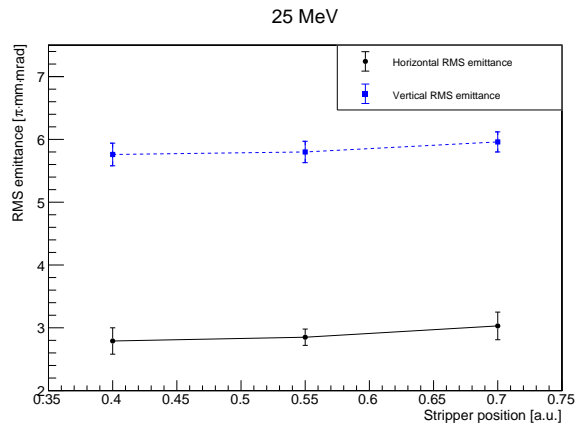


Figure 14: The RMS transverse beam emittance of the 25 MeV proton beam of the TR24 Strasbourg cyclotron as a function of stripper angular position.

183 **5. Conclusions**

184 The measurement of the transverse emittance of the beam extracted from
 185 the CYRCé TR24 cyclotron is challenging due to many parameters influenc-
 186 ing its value. Therefore, only some ranges of values and upper limits can be
 187 provided to design the new beamline. Three different methods were used. Over-
 188 all results agreed that the vertical transverse emittance was at least twice as

Table 2: RMS values of the transverse emittances (in mm.mrad) according to the method used and the beam energy (in MeV).

Method	ϵ_x	$\Delta\epsilon_x$	ϵ_y	$\Delta\epsilon_y$	Energy
Quad scan	1.90	1.30	3.70	1.40	25
Slit and grid	1.40	0.20	5.40	0.20	25
Multiple profilers	3.03	0.22	5.96	0.16	25
Multiple profilers	5.81	0.48	6.94	0.19	18

189 large as the horizontal one at a proton energy of 25 MeV (Table 2). The
190 horizontal emittance is between $\epsilon_x^{rms} = 1.40 \pm 0.20 \pi \cdot \text{mm} \cdot \text{mrad}$ and $\epsilon_x^{rms} =$
191 $3.03 \pm 0.22 \pi \cdot \text{mm} \cdot \text{mrad}$. The vertical emittance is between $\epsilon_y^{rms} = 3.70 \pm$
192 $1.40 \pi \cdot \text{mm} \cdot \text{mrad}$ and $\epsilon_y^{rms} = 5.96 \pm 0.16 \pi \cdot \text{mm} \cdot \text{mrad}$. The third method also
193 allowed to estimate upper limits of the transverse emittance at proton energy of
194 18 MeV: $\epsilon_x^{rms} \leq 5.81 \pm 0.48 \pi \cdot \text{mm} \cdot \text{mrad}$ and $\epsilon_y^{rms} \leq 6.94 \pm 0.19 \pi \cdot \text{mm} \cdot \text{mrad}$.

195 The variance of the results from the different measurements originates from
196 the accuracy of the methods, various misalignments and offsets (beam, magnets)
197 and cyclotron related (extraction from multiple orbits, cyclotron oscillations
198 etc.). Nevertheless, these measurements allowed to start the design of the new
199 beam line for radiobiology irradiations and to define the optical elements that
200 will be needed to compose it.

201 References

- 202 [1] ACSI website available at: <http://www.advancedcyclotron.com/> (ac-
203 cessed on March 29th, 2019).
- 204 [2] C. Tamburella, T. Giles, Beam diagnostics for an 18 MeV medical cy-
205 clotron, NIM B 266 (2008) 4678.
- 206 [3] A. Degiovanni et al., Emittance Measurements at the Strasbourg TR24
207 Cyclotron for the Addition of a 65 MeV Linac Booster, Proceedings of
208 Cyclotrons (2013) 329–331.

- 209 [4] H. Wiedemann, Particle Accelerator Physics, Springer 3rd Edition.
- 210 [5] Keithley Series 6400 Picoammeters, available at:
211 <https://www.tek.com/193-keithley-series-6400-picoammeters> (accessed
212 on March 29th, 2019).
- 213 [6] D. Uriot et al., TraceWin Documentation, available at:
214 <http://irfu.cea.fr/Sacm/logiciels/index3.php> (accessed on March
215 29th, 2019).
- 216 [7] K. P. Nesteruk et al., A system for online beam emittance measure-
217 ments and proton beam characterization, JINST 13 (2018) P01011,
218 arXiv:1705.07486.
- 219 [8] M. Auger et al., A detector based on silica fibers for ion beam monitoring
220 in a wide current range, JINST 11 (2016) P03027.
- 221 [9] D. E. Potkins, S. Braccini, K. P. Nesteruk, T. S. Carzaniga, A. Vedda,
222 N. Chiodini, J. Timmermans, S. Melanson, M. P. Dehnel, A Low-cost Beam
223 Profiler Based On Cerium-doped Silica Fibers, Physics Procedia 90 (2017)
224 215 – 222, conference on the Application of Accelerators in Research and
225 Industry, CAARI 2016, 30 October - 4 November 2016, Ft. Worth, TX,
226 USA.
- 227 [10] K. T. McDonald, D. P. Russell, Methods of emittance measurement, Month
228 M., Turner S. (eds) Frontiers of Particle Beams; Observation, Diagnosis and
229 Correction. Lecture Notes in Physics, Springer 343.